Nitrogen Speciation in Silicate Melts at Mantle Conditions From Ab Initio Simulations

D. Huang, J. Brodholt, P. Sossi, y. Li, M. Murakami

Geophysical Research Letters

RESEARCH LETTER
10.1029/2021GL095546

Nitrogen Speciation in Silicate Melts at Mantle Conditions From Ab Initio Simulations

D. Huang[1,2], J. Brodholt[3], P. Sossi[1], Y. Li[4,5], and M. Murakami[1]

[1]Institute of Geochemistry and Petrology, ETH Zürich, Zürich, Switzerland, [2]Institut de Physique du Globe de Paris, Paris, France, [3]Department of Earth Sciences, University College London, London, UK, [4]CAS Key Laboratory of Crust–Mantle Materials and Environments, School of Earth and Space Sciences, University of Science and Technology of China, Hefei, China, [5]CAS Center for Excellence in Comparative Planetology, University of Science and Technology of China, Hefei, China

Key Points:

- Strong N-N bonding found stable in magmas under oxidizing conditions over the entire mantle regime
- Redox conditions superimpose P and T in controlling nitrogen speciation (thus solubility) in deep magma oceans
- Nitrogen-enriched secondary atmosphere might form if the Earth accreted from sufficiently oxidized materials

Supporting Information:

Supporting Information may be found in the online version of this article.

Correspondence to:

D. Huang,
dongyang.huang@erdw.ethz.ch

Citation:

Huang, D., Brodholt, J., Sossi, P., Li, Y., & Murakami, M. (2022). Nitrogen speciation in silicate melts at mantle conditions from ab initio simulations. *Geophysical Research Letters*, *49*, e2021GL095546. https://doi.org/10.1029/2021GL095546

Received 5 AUG 2021
Accepted 7 FEB 2022

Abstract Nitrogen (N) is a major ingredient of the atmosphere, but a trace component in the silicate Earth. Its initial inventory in these reservoirs during Earth's early differentiation requires knowledge of N speciation in magmas, for example, whether it outgasses as N_2 or is sequestered in silicate melts as N^{3-}, which remains largely unconstrained over the entire mantle regime. Here we examine N species in anhydrous and hydrous pyrolitic melts at varying P-T-redox conditions by ab-initio calculations, and find N-N bonding under oxidizing conditions from ambient to lower mantle pressures. Under reducing conditions, N interacts with the silicate network or forms N-H bonds, depending on the availability of hydrogen. Redox control of N speciation is demonstrated valid over a P-T space encompassing probable magma ocean depths. Finally, if the Earth accreted from increasingly oxidized materials toward the end of its accretion, an N-enriched secondary atmosphere might be produced and persist until later impacts.

Plain Language Summary Earth's atmosphere was likely formed by the spontaneous release of gases, either from magma oceans during early Earth's accretion, or through later volcanic activity. Although our present-day atmosphere (attributed to the latter) is rich in nitrogen (N) (78%), whether this held true for the early Earth is unclear, and is determined by the species (that control the solubility) of nitrogen in the silicate melt (i.e., magma ocean). In this study, we investigate the speciation of nitrogen in silicate melts during Earth's accretion, and find that N is dissolved as N_2 at oxidizing conditions, regardless of the magma ocean's depth, promoting nitrogen degassing from the magma ocean. Our results suggest that, if Earth's building blocks were sufficiently oxidized at later times, magma ocean outgassing might produce an N-enriched atmosphere. Given the violent impact history on the early Earth, as inferred from that recorded on the surface of the Moon, atmospheric loss of N by impact erosion may provide an explanation for Earth's "missing" nitrogen.

1. Introduction

Earth's modern atmosphere is special in its nitrogen (N)-rich composition, which is likely an outcome of plate tectonics, when compared to those of Venus and Mars (Mikhail & Sverjensky, 2014). In stark contrast, the bulk silicate Earth (crust and mantle) is relatively poor in N and it occurs only in trace amounts (ppm level) (Hirschmann, 2018; Marty & Dauphas, 2003). Intriguingly, when combining the N budget of these two reservoirs, there is a well-established N anomaly in volatile elements relative to carbonaceous chondrites; although N is thought to act like noble gases during magmatic/fluid processes, it is depleted by one order of magnitude relative to other volatiles (namely, carbon, hydrogen and even the noble gases) when assuming they are present in the bulk silicate Earth in CI-chondritic ratios (Marty, 2012). The interpretation of this N deficit can be summarized in three schools of thought: (a) Its preferential incorporation into Earth's metallic core during core-mantle segregation in a magma ocean (Roskosz et al., 2013; Speelmanns et al., 2018); (b) a hitherto unsampled reservoir in the silicate mantle that takes up the the majority of N budget (Johnson & Goldblatt, 2015; Yoshioka et al., 2018); (c) early atmospheric loss by impact erosion (Genda & Abe, 2005; Tucker & Mukhopadhyay, 2014). Since it is still debated whether or not N behaves as a lithophile element during core formation (Grewal et al., 2021; Speelmanns et al., 2019), the "missing" N in the Earth remains an open question. However all the three solutions, especially the last one, raise the question of the initial inventory of N in Earth's multiple layers.

To understand the early distribution of N in terrestrial reservoirs requires knowledge of its solubility in silicate melts that make up an early magma ocean. It has been shown that nitrogen in the form of N^{3-} or N-H species is more soluble (by several orders of magnitude) than the molecular N_2 in silicate melts (Busigny & Bebout, 2013; Mysen, 2019), because the former interacts with the silicate network, whereas the latter is incorporated into the melts through interstitial occupancy (Libourel et al., 2003; Mulfinger, 1966), analogous to noble gases. Previous experiments have found that under reducing conditions, lower than IW-3 (3 log units below the iron-wüstite buffer), N mainly dissolves as N^{3-} or N-H species by interacting with silicate network or bonding with hydrogen; at moderate oxygen fugacities (fO_2), from IW-3 to IW-1.5, N-H species are dominant in hydrous silicate melts; finally, under higher fO_2 conditions (>IW-1.5), molecular N_2 becomes the primary species and hence the least compatible (Dalou et al., 2019; Grewal et al., 2020; Kadik et al., 2015; Li et al., 2015; Roskosz et al., 2006). The nitrosyl group was also proposed as a possible species under moderately oxidizing conditions (Roskosz et al., 2006). While its solubility mechanism is as yet unclear, a few experiments indicated a positive dependence of N solubility on pressure in silicate melts in equilibrium with metal (Roskosz et al., 2013). The complex speciation of N in silicate melts has received a great deal of attention; however, experimental measurements are currently limited to only shallow depths in the Earth, with the highest P-T range investigated being 6 GPa and 2473 K using a multi-anvil press (Grewal et al., 2020). The solubility and speciation at higher P-T conditions, covering the whole mantle range remains unexplored, both by experiments and theoretical calculations. Given the violent impact history and likely varying depths of magma oceans during Earth's accretion, the solubility of nitrogen under a much wider range of pressures and temperatures is required to evaluate the degree to which N was sequestered in the silicate Earth, as well as its possible atmospheric loss in the Early Earth. Here we investigate the speciation of nitrogen in pyrolitic melts from ambient conditions to ~150 GPa/4000 K, using ab initio molecular dynamics (AIMD) simulations, in order to understand its species evolution over conditions relevant to the entire mantle.

2. Methods

2.1. Supercells

A pyrolitic composition (McDonough & Sun, 1995) was chosen to approximate the bulk silicate Earth and the average magma ocean: Our initial supercell consists of 151 atoms ($Fe_4Mg_{30}Si_{24}Ca_2Al_3O_{88}$) with five oxides in pyrolitic relative proportions, without taking into account trace elements below 1 wt% (i.e., Ti, Cr, Mn, Ni, Na, K, and P) (Table SA in Data Set S1). This serves as the reference supercell and corresponds to the anhydrous and reduced end member in our simulations, with $Fe^{3+}/\sum Fe = 0$ (with 0.5 oxygen deficiency to keep the system as reduced as possible); we also designed an anhydrous and oxidized supercell by adding two oxygen atoms to raise the Fe^{3+}/Fe^{2+} ratio to 3:1 ($Fe_4Mg_{30}Si_{24}Ca_2Al_3O_{90}$). In H-bearing systems, two redox end members were simulated by adding either pure H_2 ($Fe_4Mg_{30}Si_{24}Ca_2Al_3O_{88}$+$6H_2$, reduced) or pure H_2O ($Fe_4Mg_{30}Si_{24}Ca_2Al_3O_{88}$+$6H_2O$, oxidized). Then we added 4 nitrogen atoms to the aforementioned supercells, corresponding to 1.7 wt% N in the silicate melt. In doing so, these supercells with four end-member compositions have implausibly high nitrogen fugacity (fN_2) relative to that of Earth's mantle, in which nitrogen concentration is of the order of a few parts per million (ppm) (Marty & Dauphas, 2003). Although the reference supercell has a low nominal fO_2 as fixed by its Fe^{3+}/Fe^{2+} ratio, temperature and pressure, this amount of nitrogen could actively act as an electron acceptor to effectively raise the redox conditions of the system. Due to the unavoidable limitations on the size of the supercell, it is beyond the scope of ab initio techniques to finely tune fN_2 to correlate with fO_2; hence, by removing 2 N and 2 O atoms from the reference supercell, we have designed an extremely reduced box ($Fe_4Mg_{30}Si_{24}Ca_2Al_3O_{86}$+2N). In this manner, the number of electron acceptors sufficiently decreases, producing rigorously reducing conditions under which N speciation can be examined. In total, five N-bearing supercells were considered with respect to anhydrous/hydrous and oxidized/reduced pyrolitic melts (Table S1 in Supporting Information S1). Finally, to have better statistics and to study the possible influence of N content, two additional systems were made by incorporating 8 and 16 N in the reference supercell (i.e., 3.4 and 6.6 wt%, respectively) for comparison.

2.2. Ab Initio Simulations

We performed AIMD simulations using Vienna Ab initio Simulation Package (Kresse & Hafner, 1993) based on the projector augmented wave (PAW) method (Blöchl, 1994; Kresse & Joubert, 1999). The exchange-correlation functionals were treated using the generalized gradient approximation (GGA) in the Perdew–Burke–Ernzerhof

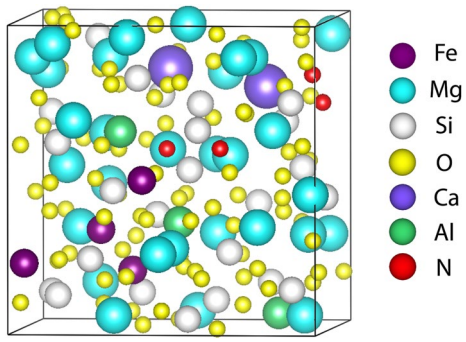

Figure 1. Snapshot from an ab initio molecular dynamics simulation with a pyrolite composition of $Fe_4Mg_{30}Si_{24}Ca_2Al_3O_{88}$ + 4N at 62 GPa and 4000 K. Among four nitrogen atoms, two of them form a strong N-N bond (red spheres, top right) which remains stable ever since its formation.

(PBE) form (Perdew et al., 1996). Valence configurations and the core radii for each element are listed in Table SA in Data Set S1. The gamma point was used to sample the Brillouin zone, with 500 eV (600 eV for H-bearing systems) cutoff energy for the plane wave expansion. Simulations at a high cutoff energy (900 eV) and a denser (2*2*2) k-point grid were run on various snapshots from each molecular dynamics (MD) run in order to estimate the Pulay stress, which was found to be less than 0.6 GPa. All the atoms in the supercell were initially randomly distributed and heated at 6000 K for at least 8 ps to obtain a well-thermalized silicate melt structure before being equilibrated at varying P-T conditions from 0.3 GPa/2000 K to 148 GPa/4000 K. The canonical ensemble with constant number of atoms (N), volume (V), and temperature (T) was used with a Nosé-Poincaré thermostat to control the temperature. Simulations were run for 13–30 ps with a time step of 1 ps for H-free or 0.5 ps for H-bearing systems. The first 1 ps was discarded and intensive variables such as P and T were calculated from the time average. If not specified otherwise, all calculations were non-spin-polarized. To examine their possible effects on speciation, we also performed spin-polarized simulations and tested + U correction in several systems, with U = 4, J = 1 (Anisimov et al., 1991; Wang et al., 2006). The influence of both on N speciation turns out to be negligible (Table SB in Data Set S1).

3. Results and Discussion

3.1. Identification of Strong N-N Bonding

We find that nitrogen atoms always manage to bond with themselves to form dimers (N_2) in relatively oxidized pyrolitic melts, despite the initial positions of all atoms being randomly assigned. In contrast N_2 species never form in the reduced melts and instead bond with the silicate network. Qualitatively this can be seen in Figure 1 which shows a snapshot taken at the end of a simulation, which was run for 15 ps at 62 GPa and 4000 K. During the first 3 ps, nitrogen diffuses through the spaces between the silicate network (Libourel et al., 2003), and mainly bonds with silicon and iron (see Movie S1 and discussions below); however, once N atoms find each other, the N-N pair persists throughout the rest of the simulation. This is observed in all of the relatively oxidized compositions, independent of whether they are hydrous or anhydrous supercells (Table S1 in Supporting Information S1).

In order to evaluate the bonding characteristics of the observed N-N species on a quantitative basis, we calculate the partial radial distribution functions (RDFs) for the equilibrated silicate melts (Figure 2). First of all, as benchmarks, the host pyrolitic melts are observed to share some common features with previously simulated silicate melts (Karki et al., 2010) with smooth and well defined first peaks (nearest neighbors) between cations and oxygen, for example, Si-O, Mg-O pairs. Although the exact location, amplitude, and shape of the cation-oxygen RDFs vary slightly under different conditions, their relative position and intensity remain unaltered in the whole investigated range of pressure, temperature and composition, as showcased in Figures 2a and 2c. This indicates that oxygen speciation is little affected by the depth or redox of the magma ocean. On the other hand, nitrogen species change readily depending on the redox state of the system, independent of the addition of hydrogen. Figure 2b shows RDFs of nitrogen, where dashed lines belong to the anhydrous and moderately oxidized end member (due to high fN_2) with a composition of $Fe_4Mg_{30}Si_{24}Ca_2Al_3O_{88}$ + 4N (see Methods) and N-N is the strongest peak. Apart from the evident N-N pair, one can readily notice the N-Si and N-Fe peaks that indicate interactions between nitrogen and the silicate network, in line with previous experiments at reducing ambient conditions (Libourel et al., 2003). In the extremely reduced melt (solid lines in Figures 2a and 2b), the N-N peak between 1.2 and 1.3 Å completely disappears and is replaced by a broader peak at 2.5 Å, which is the outcome of N incorporation into the silicate network (the second strongest peak is N-Si) and causing a decrease in its diffusivity (Table SC in Data Set S1).

The control of redox conditions on nitrogen speciation remains predominant in hydrous systems, as shown in Figures 2c and 2d, for both H_2-bearing, and H_2O-bearing melts at ~110 GPa and 4000 K. As expected, H mainly bonds with volatiles (i.e., H itself, O, and N) based on the RDF analysis. Under reducing conditions (solid lines in Figure 2d), instead of N-N in the oxidized melt (purple dashed line in Figure 2d), H-H (dark blue solid line) becomes the shortest bonding pair with a bond length of 0.76 Å, followed by O-H and N-H both at ~1 Å. As the

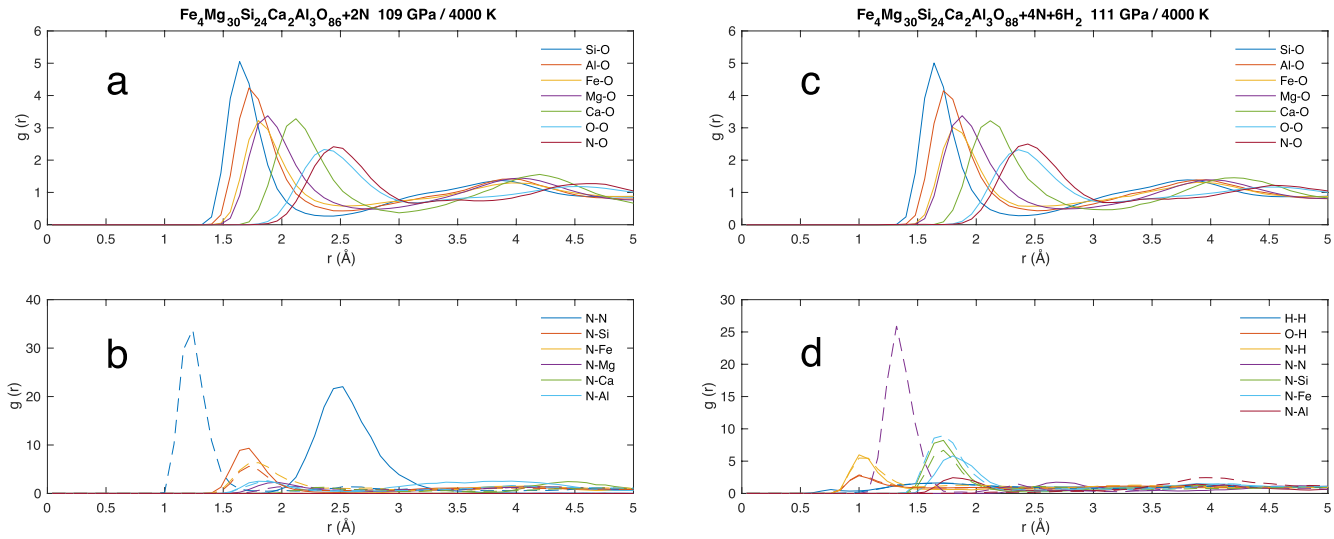

Figure 2. (a) and (b) show the partial radial distribution functions g (r) for O and N in an anhydrous and rigorously reduced melt ($Fe_4Mg_{30}Si_{24}Ca_2Al_3O_{86}$ + 2N) at 109 GPa and 4000 K. (c) and (d) show the same but with the addition of hydrogen ($Fe_4Mg_{30}Si_{24}Ca_2Al_3O_{88}$ + 4N + $6H_2$) at 111 GPa and 4000 K. Dashed lines show for comparison the N species in moderately oxidizing conditions in (b) anhydrous and (d) H_2O-bearing melts. As can be seen, reducing conditions prohibit N-N bonding, while N-N bonding is strong under oxidizing conditions.

system becomes more reduced, the N-N peak vanishes, and nitrogen mostly forms bonds with Si, Fe, and weakly with Al, which is consistent with nitride dissolution in melts under reducing conditions (Mulfinger, 1966). Under oxidizing conditions (dashed lines), the most striking observation is the emergence of the N-N peak at 1.32 Å, while all other features remain almost unaltered compared with the reduced melt, as can be seen from the overlap of solid and dashed lines (Figure 2d). It is clear that the redox conditions (i.e., the availability of electrons) control the speciation of nitrogen at pressures up to- and exceeding 100 GPa, irrespective of whether the silicate melts are anhydrous or hydrous.

Next, we consider the roles of pressure and temperature on N speciation over the entire mantle. Since it is well known that pressure and temperature can affect the redox state of a silicate melt at a given composition (Armstrong et al., 2019; Deng et al., 2020; Hirschmann, 2012), the change of P-T may alter the species of N. Nevertheless, as indicated by the RDFs in Figure S1 in Supporting Information S1, our results show that the nature of the N species is little affected by pressure and temperature in the anhydrous system ($Fe_4Mg_{30}Si_{24}Ca_2Al_3O_{88}$ + 4N), down to 1 GPa and 3000 K. Simulations at even lower temperature (2000 K) fail as the pyrolitic melt freezes. Furthermore, the insignificant P-T effect is supported by the unaltered N speciation in the hydrous system at low P-T conditions (0.3 GPa and 2000 K, Table SB in Data Set S1). Taken together, these results indicate that the N speciation change induced by P and T at a fixed composition is negligible, compared to that caused by compositional variations (namely, the amount of electron acceptors). For comparison, the RDFs for N-N pairs in two reduced melts under similar P-T conditions (taken from Figures 2b and 2d, solid lines) are shown in Figure S1 in Supporting Information S1, where the N-N peaks at ∼1.3 Å are either completely suppressed or replaced by a broader peak at a larger radius (see previous discussions). Although invisible in Figure 2 due to its relatively low intensity, a minor feature for the N-O pair is observed and plotted in Figure S2 in Supporting Information S1. The first N-O peak in RDFs between 1.3 and 1.5 Å is highly correlated with the N-N peak, both of which appear only under oxidizing conditions. This feature may provide an explanation for the experimentally observed nitrogen species that has been attributed to nitrosyl group (−NO) in relatively oxidized silicate melts (Roskosz et al., 2006).

Our simulations have not been designed to explore the potential effect of variable melt composition. Recently, high-temperature experiments performed at 1 bar found that under highly reducing conditions (IW-8), N solubility decreases with increasing degree of polymerization in silicate melts, as indicated by the value of non-bridging oxygens per tetrahedrally coordinated cation (*nbo/t*) (Mysen, 1983); however, this correlation breaks down at redox conditions relevant to early Earth's magma ocean (>IW−3.4) (Boulliung et al., 2020). In addition, because the coordination environment for Si gradually changes from tetrahedral to octahedral (Figure 3) (and

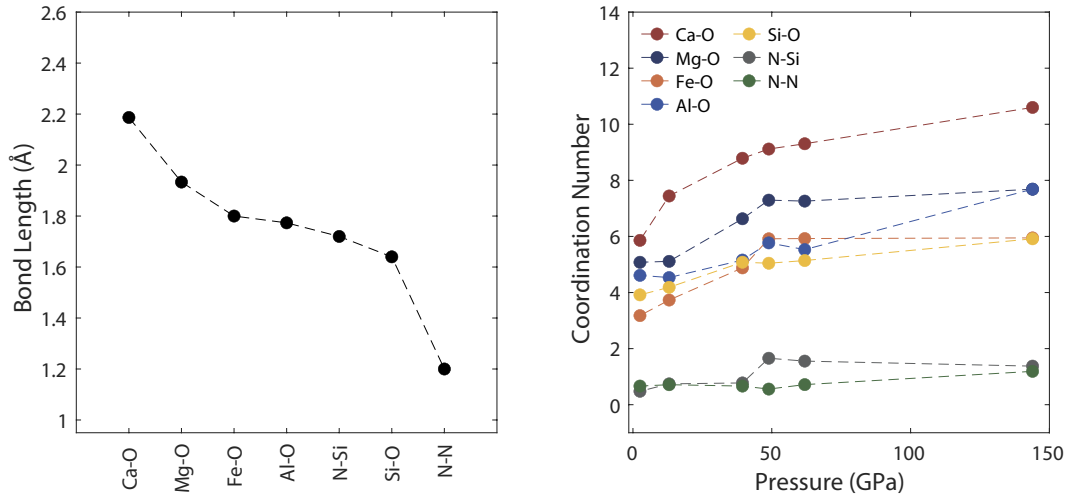

Figure 3. Bond length (Å) and coordination number for N and O species in anhydrous pyrolitic melt ($Fe_4Mg_{30}Si_{24}Ca_2Al_3O_{88}$ + 4N) at 4000 K. Note that N-N has the shortest bond length of all correlation pairs with a coordination of ∼1, indicating strong covalent bond.

other cations, such as Mg and Fe also transition to higher coordinated complexes), the *nbo/t* term is no longer an empirically adequate parameter at high pressures investigated in this study.

In summary, there is no resolvable effect of pressure and temperature on N speciation in pyrolitic melt over the entire mantle regime, and redox condition will determine N speciation over mantle conditions. Although we are not able to precisely determine the oxygen fugacity of our melts in the simulations, the speciation of N observed under varying redox conditions is qualitatively consistent with that determined by spectroscopic measurements of glasses synthesized in experiments performed at lower P-T conditions. Based on Raman spectroscopy measurements (Dalou et al., 2019; Grewal et al., 2020; Li et al., 2015; Roskosz et al., 2006), the redox conditions in those experiments, where N_2 was found to be the dominant species, would be more like our oxidized cases (including the moderately oxidized supercells); whereas the N^{3-} or NH dominated silicate melts in the experiments would be close to our reducing conditions (Table S1 in Supporting Information S1).

3.2. Silicate Melt Structure Under High Pressure

There are other properties worthy of investigation in pyrolitic melts. First, bond length between atoms can be obtained by the position in r(Å) of the first maximum of the RDF. Second, coordination number of a correlation pair can be calculated by integrating the first peak until the first minimum (details can be found in (Huang et al., 2019)). Bond lengths of O and N pairs and coordination numbers with respect to O and N calculated in this manner in the anhydrous pyrolitic melt are plotted in Figure 3. Full bond length and coordination number information are listed in Table SB in Data Set S1.

From the bond length plot, the strongest N-N peak (Figures 2a and 2b) is conspicuous in that it has the shortest mean bond length (1.2 Å) among all bonding pairs. In general, a shorter bond reflects a higher binding energy; the strong covalent bond between N-N may explain its stability once it is formed, making N_2 degassing from magma ocean feasible. As can be found in Table SB in Data Set S1, the bond length of most neighbors varies little with pressure, with the exception of O-O, whose bond distance decreases gradually from 2.76 Å at 3 GPa to 2.28 Å at 144 GPa. This means that the compression of silicate melt occurs primarily via the densification of O atoms, which is manifest in an increase in the mean coordination numbers of cations (Si, Mg, Fe, etc.) with respect to O (Figure 3). In the right panel of Figure 3, all the cations' coordination numbers with respect to oxygen increase as the melt is being pressurized. For instance, C_{SiO} changes from four to six, that is, the bonding polyhedra in the silicate network transform from tetrahedra to octahedra (Sanloup et al., 2013; Stixrude & Karki, 2005); neighboring O number increases from 6 to ∼11 for Ca, 5 to 8 for Mg, 2 to 6 for Fe, and 5 to 8 for Al, from 3 to 144 GPa. On the other hand, C_{NN} (Figure 3, right panel) fluctuates between 0.7 and 1.2, close to unity, which indicates the formation of N_2 molecules.

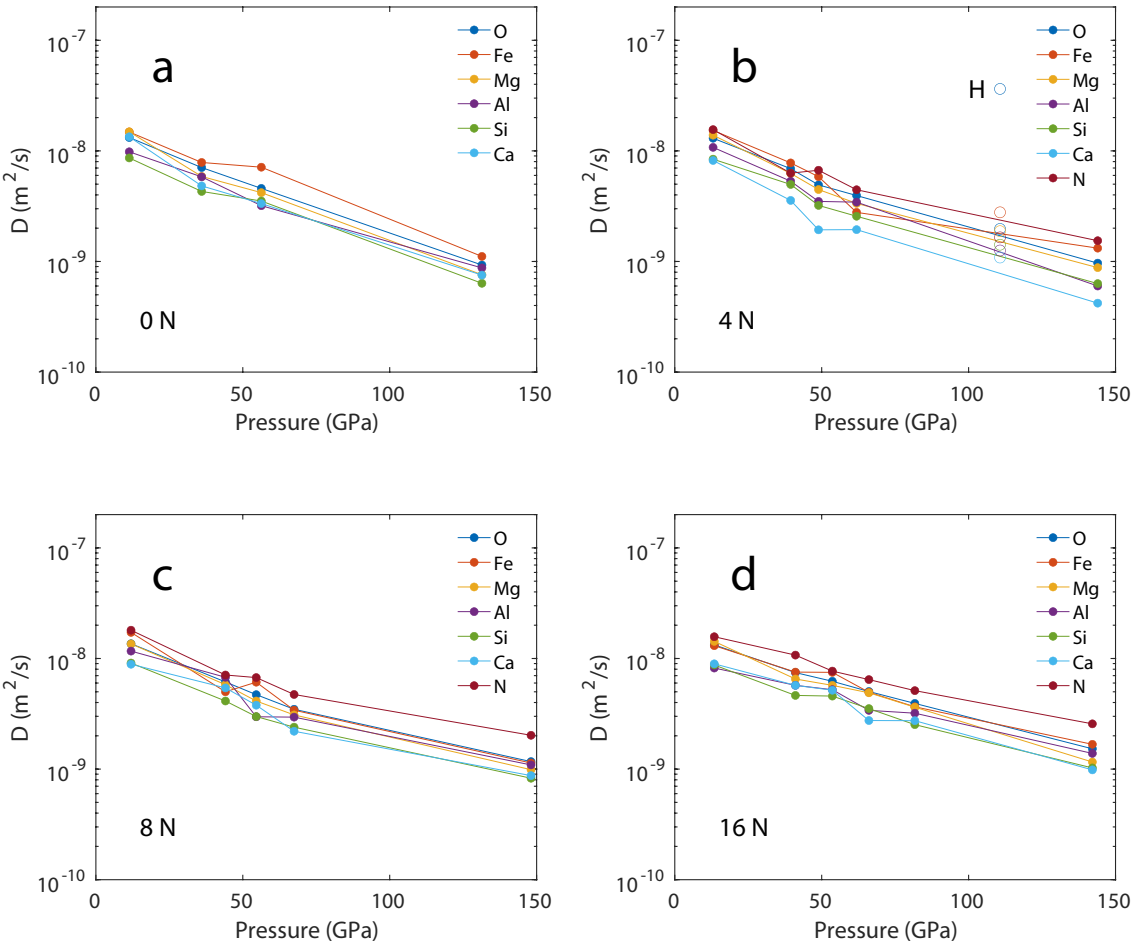

Figure 4. Self-diffusion coefficient *D* for all elements in mantle pressure range at 4000 K in pyrolitic melts with (a) no N, (b) 1.7 wt% N (4 N), (c) 3.4 wt% N (8 N), and (d) 6.6 wt% N (16 N). For comparison, the *D*s for hydrous/reduced silicate melt (pyrolite + 4N + $6H_2$) are plotted as open circles in (b). Except for N, elements listed in the legend roughly follow a descending diffusion rate.

3.3. Diffusivity in Silicate Melt: Possible Influence of Volatiles

Self-diffusion coefficients for the elements in pyrolitic melts with various N contents are reported in Figure 4. Under a given set of P-T conditions, all elements, except hydrogen, exhibit similar diffusivities within one order of magnitude of one another, ranging between 10^{-8} at the lowest pressures to 10^{-9} m^2/s at ~150 GPa, consistent with previous calculations (Karki et al., 2010). As expected, at deeper magma ocean depth, pressure uniformly suppresses the diffusion of all species: this negative correlation between diffusivity and pressure is best demonstrated in Figure 4. The addition of nitrogen very slightly increases the overall diffusivity for all the elements investigated here: For instance at ~140 GPa, the *D*s collectively shift upwards from below to above 10^{-9} m^2/s with increasing N content (Figures 4a–4d). This effect of nitrogen content on diffusivity is more pronounced at high pressures, for example, as shown in Figure S3 in Supporting Information S1, where D_N positively correlates with N content in silicate melts at a given pressure, and this correlation is more evident at higher pressures. However, these melts have very high concentrations of N and so N would not be expected to affect diffusion rates in natural pyrolitic melts. The presence of H, on the other hand, seems to exert no resolvable influence on other elements' diffusivities, because their calculated self-diffusion rates in H-bearing melts closely follow the trends in Figure 4b.

Note that network-forming cations Si (green dots in Figure 4) have lower diffusion coefficients than network modifiers, such as Mg (yellow dots). Calcium (light blue dots), on the other hand, has a very low diffusivity, likely controlled by its intrinsic properties (e.g., large atomic radius) (Ni et al., 2015). In agreement with previous simulations on silicate melts (Karki et al., 2010; Solomatova et al., 2019), the diffusion coefficients of Fe, Mg,

and O are nearly indistinguishable (the differences are well below a factor of two, Table SC in Data Set S1) at all pressures. Hydrogen is the smallest and the lightest atom, and therefore possesses the highest diffusion rate (open circle, Figure 4b); similarly, N the second highest diffusivity (crimson spheres, Figures 4b–4d). Under oxidizing conditions, N forms stable bonds with itself and has a high mobility in silicate melts; due to the low solubility of N_2, its high diffusivity would again facilitate the gas-melt phase separation during magma outgassing, rather than its sequestration in the mantle.

4. Implications for Earth's Secondary Atmosphere and N Deficit

The N-N bonding observed in pyrolitic melt, provided conditions are sufficiently oxidized, would conceivably promote the degassing of nitrogen at the surface of the magma ocean, owing to the lower solubility of N_2 with respect to N^{3-} (Bernadou et al., 2021; Boulliung et al., 2020; Libourel et al., 2003). We demonstrate that the N_2 speciation observed under oxidizing conditions in experimentally-synthesized basaltic melts also holds for a peridotitic mantle representative of the Earth. Therefore, solubility relationships derived from these studies are expected to be applicable to reconciling the behavior of N during Earth's accretion. What follows is a qualitative discussion of the fate of N given the prevailing accretion models and the variation of oxygen fugacity that they entail. Although the redox path through which the Earth evolved is debated (Huang et al., 2020; Rubie et al., 2015; Siebert et al., 2013; Sossi et al., 2020; Wood et al., 2008), with due precautions, one can make some first-order deductions. If we take the most plausible scenario, that is, Earth's accretion sampled initially reduced and subsequently oxidized material, depending on the timing of volatile delivery to the inner solar system, three possibilities are viable regarding the fate of nitrogen in the Earth. (a) If volatiles, including nitrogen, are accreted through major stages of Earth's formation (Halliday, 2013), nitrogen degassing would occur only later as fO_2 increases; in this way, a certain amount of N could be trapped in the mantle (or core, depending on its partition coefficient into metal). (b) If volatiles come later to the Earth, that is, through heterogeneous accretion (e.g., (Huang et al., 2021; Rubie et al., 2015; Schönbächler et al., 2010)), because of higher fO_2, an N-enriched secondary atmosphere might accumulate during the later stages of Earth's growth. (c) Some volatiles might also be delivered by the so-called “late veneer” after planets achieved their final masses (Albarède, 2009); however, since this process requires no magma ocean, our simulations are not able to assess the fate of N in this case. Nevertheless, the first scenario (homogeneous accretion) is compatible with the view that Earth's missing nitrogen might well be sequestered and isolated in the mantle or core through geological time, whereas the heterogeneous accretion scenario permits models in which early impactors induce loss of an N-enriched atmosphere. Both scenarios may represent plausible explanations for Earth's N deficit. An alternative redox path, where Earth's formation started in oxidizing and ended up with reducing conditions (Huang et al., 2020; Siebert et al., 2013), may also be reconciled with Earth's N budget when one envisages N_2 degassing and subsequent atmospheric loss by impacts take place from early stages of accretion.

5. Conclusions

Based on atomic trajectory and the analysis of N speciation (partial radial distribution function, bond length, and coordination number), strong N-N bonding is observed in oxidized pyrolitic melts over mantle pressure range. Under truly reducing conditions, N becomes part of the silicate network by bonding with Si (and H in hydrous melts). These findings are consistent with previous ambient to lower pressure experiments. Of all the thermodynamic parameters, we find redox state to be the factor controlling N speciation, whereas pressure and temperature mainly affect other physical properties, including bond length (melt density), coordination number (melt structure), and diffusivity (melt viscosity). Hydrogen tends to bond with volatiles (H, O, and N) and has the highest diffusion rate of all elements examined here. The presence of nitrogen slightly increases the overall diffusivity of silicate melt components under high pressures. Finally, if volatiles were delivered together with materials with increasing oxygen fugacity toward the end of Earth's accretion, an N-enriched secondary atmosphere might form and be blown away by subsequent impacts, thus accounting for the N deficit in Earth's mantle.

Data Availability Statement

Ab initio molecular dynamics data are available in the repository Mendeley Data with https://doi.org/10.17632/hkzm3prfdt.1.

Acknowledgments
We are grateful to Guillaume Avice for helpful discussions. We thank Yuan Li and an anonymous reviewer for their constructive comments and Steven Jacobsen for handling this manuscript. The research leading to these results was supported by NERC grant NE/M015181/1 and NE/S01134X/1. M. Murakami acknowledges support from the ETH startup funding. PAS was supported by an SNF Ambizione fellowship (No. 180025). Simulations were performed using the ARCHER UK National Supercomputing Service. Open access funding provided by Eidgenossische Technische Hochschule Zurich.

References

Albarède, F. (2009). Volatile accretion history of the terrestrial planets and dynamic implications. *Nature*, *461*(7268), 1227–1233. https://doi.org/10.1038/nature08477

Anisimov, V. I., Zaanen, J., & Andersen, O. K. (1991). Band theory and Mott insulators: Hubbard U instead of Stoner I. *Physical Review B*, *44*(3), 943–954. https://doi.org/10.1103/PhysRevB.44.943

Armstrong, K., Frost, D. J., McCammon, C. A., Rubie, D. C., & Boffa Ballaran, T. (2019). Deep magma ocean formation set the oxidation state of Earth's mantle. *Science*, *365*(6456), 903–906. https://doi.org/10.1103/PhysRevB.50.17953

Bernadou, F., Gaillard, F., Füri, E., Marrocchi, Y., & Slodczyk, A. (2021). Nitrogen solubility in basaltic silicate melt—Implications for degassing processes. *Chemical Geology*, *573*, 120192. https://doi.org/10.1016/j.chemgeo.2021.120192

Blöchl, P. E. (1994). Projector augmented-wave method. *Physical Review B: Condensed Matter*, *50*, 17953–17979. https://doi.org/10.1103/PhysRevB.50.17953

Boulliung, J., Füri, E., Dalou, C., Tissandier, L., Zimmermann, L., & Marrocchi, Y. (2020). Oxygen fugacity and melt composition controls on nitrogen solubility in silicate melts. *Geochimica et Cosmochimica Acta*, *284*, 120–133. https://doi.org/10.1016/j.gca.2020.06.020

Busigny, V., & Bebout, G. E. (2013). Nitrogen in the silicate Earth: Speciation and isotopic behavior during mineral-fluid interactions. *Elements*, *9*(5), 353–358. https://doi.org/10.2113/gselements.9.5.353

Dalou, C., Hirschmann, M. M., Jacobsen, S. D., & Le Losq, C. (2019). Raman spectroscopy study of C-O-H-N speciation in reduced basaltic glasses: Implications for reduced planetary mantles. *Geochimica et Cosmochimica Acta*, *265*, 32–47. https://doi.org/10.1016/j.gca.2019.08.029

Deng, J., Du, Z., Karki, B. B., Ghosh, D. B., & Lee, K. K. M. (2020). A magma ocean origin to divergent redox evolutions of rocky planetary bodies and early atmospheres. *Nature Communications*, *11*(1). https://doi.org/10.1038/s41467-020-15757-

Genda, H., & Abe, Y. (2005). Enhanced atmospheric loss on protoplanets at the giant impact phase in the presence of oceans. *Nature*, *433*(7028), 842–844. https://doi.org/10.1038/nature03360

Grewal, D. S., Dasgupta, R., & Farnell, A. (2020). The speciation of carbon, nitrogen, and water in magma oceans and its effect on volatile partitioning between major reservoirs of the solar system rocky bodies. *Geochimica et Cosmochimica Acta*, *280*, 281–301. https://doi.org/10.1016/j.gca.2020.04.023

Grewal, D. S., Dasgupta, R., Hough, T., & Farnell, A. (2021). Rates of protoplanetary accretion and differentiation set nitrogen budget of rocky planets. *Nature Geoscience*, *14*(6), 369–376. https://doi.org/10.1038/s41561-021-00733-0

Halliday, A. N. (2013). The origins of volatiles in the terrestrial planets. *Geochimica et Cosmochimica Acta*, *105*, 146–171. https://doi.org/10.1016/j.gca.2012.11.015

Hirschmann, M. M. (2012). Magma ocean influence on early atmosphere mass and composition. *Earth and Planetary Science Letters*, *341–344*, 48–57. https://doi.org/10.1016/j.epsl.2012.06.015

Hirschmann, M. M. (2018). Comparative deep Earth volatile cycles: The case for C recycling from exosphere/mantle fractionation of major (H_2O , C, N) volatiles and from H_2O/Ce , CO_2/Ba , and CO_2/Nb exosphere ratios. *Earth and Planetary Science Letters*, *1*, 1–12. https://doi.org/10.1016/j.epsl.2018.08.023

Huang, D., Badro, J., Brodholt, J., & Li, Y. (2019). Ab initio molecular dynamics investigation of molten Fe–Si–O in Earth's core. *Geophysical Research Letters*, *46*(12), 6397–6405. https://doi.org/10.1029/2019GL082722

Huang, D., Badro, J., & Siebert, J. (2020). The niobium and tantalum concentration in the mantle constrains the composition of Earth's primordial magma ocean. *Proceedings of the National Academy of Sciences*, 117(45), 27893–27898. https://doi.org/10.1073/pnas.2007982117

Huang, D., Siebert, J., & Badro, J. (2021). High pressure partitioning behavior of Mo and W and late sulfur delivery during Earth's core formation. *Geochimica et Cosmochimica Acta*, *310*, 19–31.

Johnson, B., & Goldblatt, C. (2015). The nitrogen budget of Earth. *Earth-Science Reviews*, *148*, 150–173. https://doi.org/10.1016/j.earscirev.2015.05.006

Kadik, A. A., Koltashev, V. V., Kryukova, E. B., Plotnichenko, V. G., Tsekhonya, T. I., & Kononkova, N. N. (2015). Solubility of nitrogen, carbon, and hydrogen in FeO–Na_2O–Al_2O_3–SiO_2 melt and liquid iron alloy: Influence of oxygen fugacity. *Geochemistry International*, *53*(10), 849–868. https://doi.org/10.1134/S001670291510002X

Karki, B. B., Bhattarai, D., Mookherjee, M., & Stixrude, L. (2010). Visualization-based analysis of structural and dynamical properties of simulated hydrous silicate melt. *Physics and Chemistry of Minerals*, *37*(2), 103–117. https://doi.org/10.1007/s00269-009-0315-1

Kresse, G., & Hafner, J. (1993). Ab initio molecular dynamics for liquid metals. *Physical Review B*, *47*(1), 558. https://doi.org/10.1103/PhysRevB.47.558

Kresse, G., & Joubert, D. (1999). From ultrasoft pseudopotentials to the projector augmented-wave method. *Physical Review B: Condensed Matter and Materials Physics*, *59*(3), 1758–1775. https://doi.org/10.1103/PhysRevB.59.1758

Li, Y., Huang, R., Wiedenbeck, M., & Keppler, H. (2015). Nitrogen distribution between aqueous fluids and silicate melts. *Earth and Planetary Science Letters*, *411*, 218–228. https://doi.org/10.1016/j.epsl.2014.11.050

Libourel, G., Marty, B., & Humbert, F. (2003). Nitrogen solubility in basaltic melt. Part I. Effect of oxygen fugacity. *Geochimica et Cosmochimica Acta*, *67*(21), 4123–4135. https://doi.org/10.1016/S0016-7037(03)00259-X

Marty, B. (2012). The origins and concentrations of water, carbon, nitrogen and noble gases on Earth. *Earth and Planetary Science Letters*, *313–314*(1), 56–66. https://doi.org/10.1016/j.epsl.2011.10.040

Marty, B., & Dauphas, N. (2003). The nitrogen record for crust-mantle interaction and mantle convection from Archean to present. *Earth and Planetary Science Letters*, *206*(3–4), 397–410. https://doi.org/10.1016/S0012-821X(02)01108-1

McDonough, W., & Sun, S.-s. (1995). The composition of the Earth. *Chemical Geology*, *120*(3), 223–253. https://doi.org/10.1016/0009-2541(94)00140-4

Mikhail, S., & Sverjensky, D. A. (2014). Nitrogen speciation in upper mantle fluids and the origin of Earth's nitrogen-rich atmosphere. *Nature Geoscience*, *7*(11), 816–819. https://doi.org/10.1038/ngeo2271

Mulfinger, H.-O. (1966). Physical and chemical solubility of nitrogen in glass melts. *Journal of the American Ceramic Society*, *49*(9), 462–467. https://doi/org/10.1111/j.1151-2916.1966.tb13300.x

Mysen, B. (1983). The Structure of silicate melts. *Annual Review of Earth and Planetary Sciences*, *11*, 75–97. https://doi.org/10.1248/cpb.10.879

Mysen, B. (2019). Nitrogen in the Earth: Abundance and transport. *Progress in Earth and Planetary Science*, *6*(38), 1–15. https://doi.org/10.1186/s40645-019-0286-x

Ni, H., Hui, H., & Steinle-Neumann, G. (2015). Transport properties of silicate melts. *Reviews of Geophysics*, *53*(3), 715–744. https://doi.org/10.1002/2015RG000485

Perdew, J. P., Burke, K., & Ernzerhof, M. (1996). Generalized gradient approximation made simple. *Physical Review Letters*, *77*, 3865–3868. https://doi.org/10.1103/PhysRevLett.77.3865

Roskosz, M., Bouhifd, M. A., Jephcoat, A. P., Marty, B., & Mysen, B. O. (2013). Nitrogen solubility in molten metal and silicate at high pressure and temperature. *Geochimica et Cosmochimica Acta*, *121*, 15–28. https://doi.org/10.1016/j.gca.2013.07.007

Roskosz, M., Mysen, B. O., & Cody, G. D. (2006). Dual speciation of nitrogen in silicate melts at high pressure and temperature: An experimental study. *Geochimica et Cosmochimica Acta*, *70*(11), 2902–2918. https://doi.org/10.1016/j.gca.2006.03.001

Rubie, D. C., Jacobson, S. A., Morbidelli, A., Brien, D. P. O., Young, E. D., Vries, J. D., et al. (2015). Accretion and differentiation of the terrestrial planets with implications for the compositions of early-formed solar system bodies and accretion of water. *ICARUS*, *248*, 89–108. https://doi.org/10.1016/j.icarus.2014.10.015

Sanloup, C., Drewitt, J. W. E., Konôpková, Z., Dalladay-Simpson, P., Morton, D. M., Rai, N., et al. (2013). Structural change in molten basalt at deep mantle conditions. *Nature*, *503*(7474), 104–107. https://doi.org/10.1038/nature12668

Schönbächler, M., Carlson, R. W., Horan, M. F., Mock, T. D., & Hauri, E. H. (2010). Heterogeneous accretion and the moderately volatile element budget of Earth. *Science*, *328*(5980), 884–887. https://doi.org/10.1126/science.1186239

Siebert, J., Badro, J., Antonangeli, D., & Ryerson, F. J. (2013). Terrestrial accretion under oxidizing Conditions. *Science*, *339*(6124), 1194–1197. https://doi.org/10.1126/science.1227923

Solomatova, N. V., Caracas, R., & Manning, C. E. (2019). Carbon sequestration during core formation implied by complex carbon polymerization. *Nature Communications*, *10*(1). https://doi.org/10.1038/s41467-019-08742-9

Sossi, P. A., Burnham, A. D., Badro, J., Lanzirotti, A., Newville, M., & O'Neill, H. S. (2020). Redox state of Earth's magma ocean and its venus-like early atmosphere. *Science Advances*, *6*(48). https://doi.org/10.1126/sciadv.abd1387

Speelmanns, I. M., Schmidt, M. W., & Liebske, C. (2018). Nitrogen solubility in core materials. *Geophysical Research Letters*, *45*(15), 7434–7443. https://doi.org/10.1029/2018GL079130

Speelmanns, I. M., Schmidt, M. W., & Liebske, C. (2019). The almost lithophile character of nitrogen during core formation. *Earth and Planetary Science Letters*, *510*, 186–197. https://doi.org/10.1016/j.epsl.2019.01.004

Stixrude, L., & Karki, B. (2005). Structure and freezing of $MgSiO_3$ liquid in Earth's lower mantle. *Science*, *310*(5746), 297–299. https://doi.org/10.1126/science.1116952

Tucker, J. M., & Mukhopadhyay, S. (2014). Evidence for multiple magma ocean outgassing and atmospheric loss episodes from mantle noble gases. *Earth and Planetary Science Letters*, *393*, 254–265. https://doi.org/10.1016/j.epsl.2014.02.050

Wang, L., Maxisch, T., & Ceder, G. (2006). Oxidation energies of transition metal oxides within the GGA+U framework. *Physical Review B: Condensed Matter and Materials Physics*, *73*(19), 1–6. https://doi.org/10.1103/PhysRevB.73.195107

Wood, B. J., Wade, J., & Kilburn, M. R. (2008). Core formation and the oxidation state of the Earth: Additional constraints from Nb, V and Cr partitioning. *Geochimica et Cosmochimica Acta*, *72*(5), 1415–1426. https://doi.org/10.1016/j.gca.2007.11.036

Yoshioka, T., Wiedenbeck, M., Shcheka, S., & Keppler, H. (2018). Nitrogen solubility in the deep mantle and the origin of Earth's primordial nitrogen budget. *Earth and Planetary Science Letters*, *488*, 134–143. https://doi.org/10.1016/j.epsl.2018.02.021

Reference From the Supporting Information

Stixrude, L., Scipioni, R., & Desjarlais, M. P. (2020). A silicate dynamo in the early Earth. *Nature Communications*, *11*(1). https://doi.org/10.1038/s41467-020-14773-4